Impact of the Voltage and Frequency of a Pulse Signal Applied to a Toroidal Coil on Near Magnetic Field Measurements

Abdelhakim Zeghoudi[1], Abdelber Bendaoud[1], Seyf Eddine Bechekir[2]

Abstract: In power electronic systems, electromagnetic radiation of the near field is detrimental because it generates electromagnetic interference in static converters ultimately leading to the degradation of the EMC filter performance. This paper presents an experimental investigation into magnetic radiation generated by magnetic components, specifically toroidal inductors, in the time domain (TD) using an oscilloscope and in the frequency domain (FD) via a spectrum analyzer. The method employed to quantify the magnetic field is the near field scan (NFS) using magnetic probes. This approach enables us to identify the areas with the highest magnetic field emissions from the toroidal inductance across its three components (H_X, H_Y, H_Z). Initially, our investigation focused on two key parameters of the pulse signal. First, we examined the impact of varying the pulse signal's frequency while keeping the voltage constant. Next, we analyzed the effect of variations in the amplitude of the pulse signal while keeping a constant frequency. Following these experiments, we generated magnetic field maps in the frequency domain (FD) above the surface of the inductor, specifically focusing on the H_Z component. The scanning step is equal to 0,5 cm. The scanning area is equal to $(x, y) = (4 \text{ cm}, 4 \text{ cm})$.

Keywords: Toroidal inductor, Scanning near magnetic field, Time domain (TD), pulse signal, Frequency domain (FD).

1   Introduction

The inductor is a fundamental and indispensable component for power electronics circuits. It is used for example in electrical energy conversion, where it serves as a storage element or in switching power supplies. It is also used in the realization of EMC filters and in low noise amplifiers [1]. However, the

---

[1]Laboratory of Applications of Plasma, Electrostatics and Electromagnetic Compatibility (APELEC) Faculty of Electrical Enginnering, DjillaliLiabesUniversityof Sidi Bel-Abbès, Sidi Bel-Abbès 22000, Algeria, E-mail: Abdelhakim.zeghoudi@univ-sba.dz, babdelber@gmail.com

[2]Laboratory of Intelligent Control and Electrical Power System (ICEPS), Faculty of Electrical Enginnering, Djillali Liabes University of Sidi Bel-Abbès, Sidi Bel-Abbès 22000, Algeria E-mail: seyfeddine.electrotechnique@gmail.com

challenges posed by inductors are numerous: they exhibit non-linear behavior, necessitate more complex micro-fabrication processes and emit electromagnetic radiations, notably in the form of magnetic field. Numerous works have been devoted to the quantification of the magnetic field produced by an inductor. Some authors have focused on devising test benches for the characterization of radiated emissions [2 − 5], while others have delved into [6] exploring the coupling between the inductor and the neighboring component. Additionally, some authors have shown interest in comparing the radiated fields emitted by inductors of varying shapes [7].

In the realm of power electronic systems, magnetic components, including inductors and transformers, stand out as primary sources of radiated emissions in the form of magnetic fields. The experimental results presented in [9 − 13] prove that radiated emissions emitted by magnetic components can increase EMI and degrade the filter performance. Hariya et al. [14] have shown that the magnetic field emitted by a transformer could increase the current power loss.

Furthermore, the endeavor to quantify magnetic fields in integrated circuits and converters has gained significant traction. Certain researchers have dedicated their efforts to modeling and analyzing electromagnetic radiation within the context of an Automotive Non-isolated Power Converter [15 − 19]. Some authors developed and analyzed the near magnetic field in rectangular capacitors [20]. The authors in [21 − 24] propose a characterization method to evaluate EM disturbances in the near field for electronic systems.

The objective of this paper is to quantify the near magnetic field emitted by the toroidal inductor in both the Time Domain (TD) and Frequency Domain (FD). To achieve this objective, we employed an oscilloscope (modelGDS-3352 Gw INSTEK) for TD analysis and a spectrum analyzer (model ANRITSU MS2830A-6GHz) for the FD analysis. Additionally, we validate the consistency of results between these two domains using the near-field scan technique with Rohde Schwarz magnetic field probes. Firstly, it is necessary to assess the high-frequency behavior of the studied inductor. This evaluation was conducted using an impedance analyzer (type 20 Hz-120 MHz serial 6500B WAYNE KRR Electronics). The signal applied to the inductor's terminals takes the form of pulses, generated using a low-frequency generator (model Diglent SDG 1025 25MHz). The signal is varied in two ways: once by varying the frequency, and the other time by varying the voltage amplitude. These variations are intended to provide insight into the impact of frequency and voltage on the magnetic field of all the components as measured by the near magnetic field probes of the Rohde Schwarz type.

In this context, this paper is organized as follows: Section II presents the studied circuit, which comprises a toroidal inductor fed by a pulse signal. This signal is applied in two different scenarios: once with variable frequency and

fixed amplitude, and the other time, with a fixed frequency and varying voltage. In Section III, the method for near-field scanning in both the time domain (TD) and frequency domain (FD) is elaborated upon. This is achieved using an oscilloscope for TD analysis and a spectrum analyzer for FD analysis. The magnetic probe employed for these measurements is of the RSH-50-1 (Rohde Schwarz type). In Section IV, the results obtained from the near magnetic field experiments in both domains are presented. The purpose of this section is to facilitate a comparison between the two domains. Additionally, it delves into elucidating the impact of varying the frequency and voltage of the pulse signal applied to the inductor's terminals on the magnetic emissions. The conclusion is presented in Section V. The research was carried out in the laboratory "Application of plasma, Electrostatics, Electromagnetic Compatibility (APELEC)" at Djilali Liabès University of Sidi Bel-Abbès.

2   Study of Toroidal Coils

An inductor is a passive component that stores energy in the form of a magnetic field. This winding is usually made around a magnetic material or a set of materials forming the magnetic circuit in order to channel the magnetic field, reduce losses and increase the value of the inductance. The value of the inductance depends on the number of turns, the geometry and the surrounding materials [25]. Fig. 1 shows the toroidal coil studied in this work. The number of turns is 47, core Material iron powder, outside diameter: 12,7 mm, internal diameter: 7,7 mm, Length: 4,83 mm, Density: 7.0 cm³, Curie temperature: 825 °C, Density: 7.0 cm³, Permeability: 75 µo.

Fig. 1 – *Photograph of the studied inductor.*

Fig. 2 shows the photograph of the bench used for measuring the behavior of inductance (impedance, and phase) using the impedance analyzer as a function of frequency in a range [100 Hz – 30MHz].
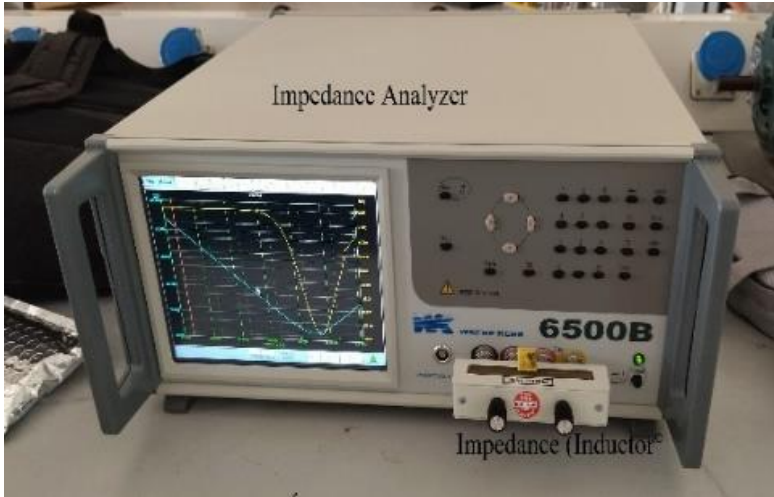
Fig. 2 – *Photograph of the bench used for measuring the behavior of the inductor.*

Fig. 3 shows the model of the real inductor under study at high frequencies, comprised of a self-inductance L_{pr} and an internal resistance R_s, in parallel with a parasite capacitance C_p.
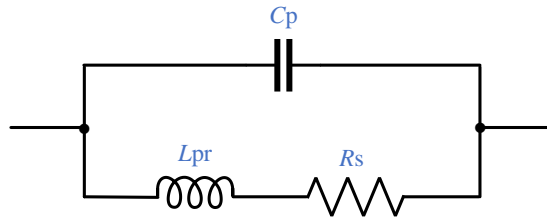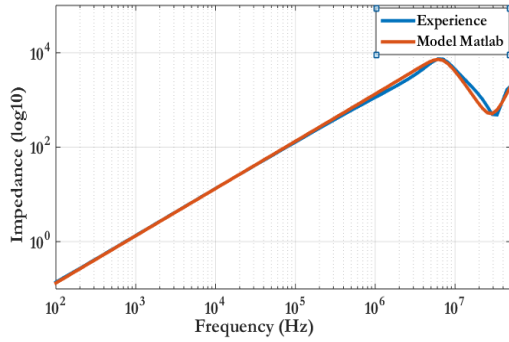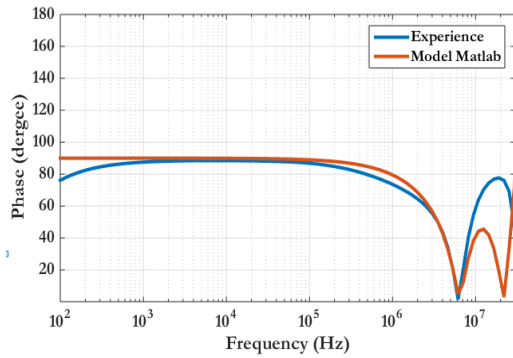

Fig. 3 *– Equivalent model of the real inductor under study at high frequency.*

In Fig. 4, we show the frequency variations of the impedance of an inductance whose value $L = 221$ μH, obtained through modeling in Matlab software and experimentation using an impedance analyzer. We can see a concordance between the results of modeling and experimentation. Specifically, at low frequencies, the impedance of the inductance matches the internal resistance. As shown in Fig. 4a, as the frequency increase, the impedance of the inductance starts to increase linearly until it reaches the resonant frequency denoted as f_0, with a value of 7 MHz (impedance peak). At this point, inductance and the parasitic capacitance C_{pr} resonate. As the frequency increases beyond the resonance frequency, the impedance of the parasitic capacitance decreases resulting in a decrease in the impedance of the real inductor.

(a)

(b)

Fig. 4 – *Diagram of the equivalent model of the real high frequency inductance:* (a) *Impedance;* (b) *Phase.*

3 Scan of Near Field in the Time and Frequency Domains

When studying the radiation of an electromagnetic source, the concept of radiated field is introduced. We distinguish two areas of electromagnetic field: the area of near field and the area of far field [26], as shown in Fig. 5.
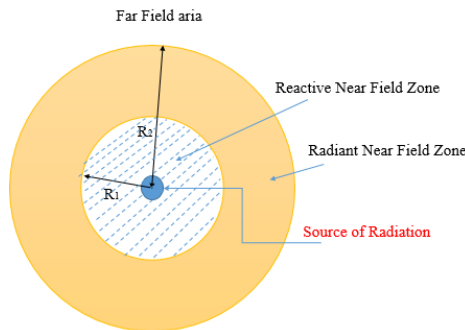

Fig. 5 – *Description of the field areas around a radiation source* [27].

411

In our study, we measure the near magnetic field generated by electronic components such as an inductor by magnetic loop probes.

Fig. 6 shows a photograph of the bench used for near magnetic field measurement in the frequency domain, employing the RSH-50-1 probe of the Rohde Schwarz type. The frequency measurement method uses a high precision spectrum analyzer that has a wide bandwidth. This analyzer is utilized to display and record the frequency signals captured by the measurement of the magnetic field probe. When using a spectrum analyzer to measure a magnetic field, the specific limits and probabilities would depend on factors such as the sensitivity and dynamic range of the spectrum analyzer, as along with the characteristics of the magnetic field under examination. The datasheet of the coaxial cable specifies an attenuation of 0.5 dB/m at the frequency range of interest. Therefore, the total attenuation introduced by the cable would be 0.5 dB/m $\times$ 1 m = 0.5 dB. It is noteworthy that the spectrum analyzer is designed for RF (Radio Frequency) measurements in the frequency range of 10 Hz to 6 GHz. This spectrum analyzer has a resolution bandwidth of 1 MHz and a specified amplitude accuracy of $\pm$1 dB.
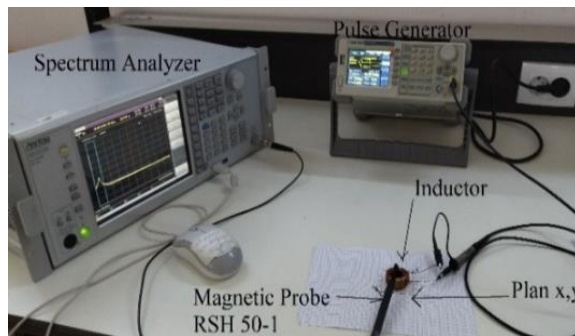

Fig. 6 – *Photograph of the bench measuring the near magnetic field above the inductor in the frequency domain.*

Fig. 7 illustrates a descriptive diagram of different parts of the near field test bench. The movement of the probe over the structure studied is done manually. The procedure involves moving the probe from one measurement point to another on the scanning surface with a step of 0.5 cm.

Fig. 8 shows a photograph of the near magnetic field measurement bench using the RSH-50-1 probe of the Rohde Schwarz type in the time domain (TD). The time measurement method uses an oscilloscope, which is used to display and record the time signals captured by the magnetic field probe measurement.

Fig. 9 shows a descriptive diagram of the various parts of the near field test bench. The movement of the probe over the structure under study is done manually and the scanning step over the surface of the inductor is equal to 0.5 cm as shown in Fig. 6.
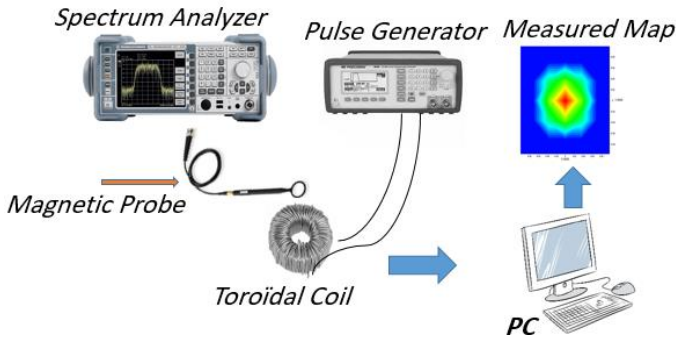
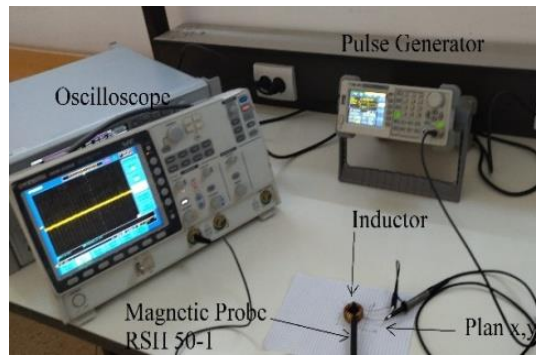**Fig. 7** – *Descriptive diagram of near magnetic field measurement in frequency domain.*

Fig. 8 – *Photograph of the bench measuring the near magnetic field above the toroidal inductor in the time domain.*

The magnetic field probe RS H 50-1 (diameter about 10 mm) is well-suited for measurements at a smaller distance, up to about 3 cm. Within this range, it enables a more precise determination of the distribution and orientation of the field [28]. Fig. 10 depicts the probe used for measuring the near magnetic field in our work. The detector employed is a coil detector designed to detect variations in magnetic flux, with a bandwidth ranging from 0 to 500 MHz.

To measure the magnetic fields around electrical components and electronic systems, we can use magnetic probes, and to capture the different components of the magnetic field H. These probes are positioned with their normal aligned with the surface of the loop of the component under investigation. A single probe can be reoriented as needed depending on the component being measured. The underlying principle of the measurement protocol is based on Faraday and Lenz's law, which states that a varying magnetic field $F(t)$ passing through a closed circuit induces an electromotive force "e" across the loop. Expression (1) shows Faraday's law [29].
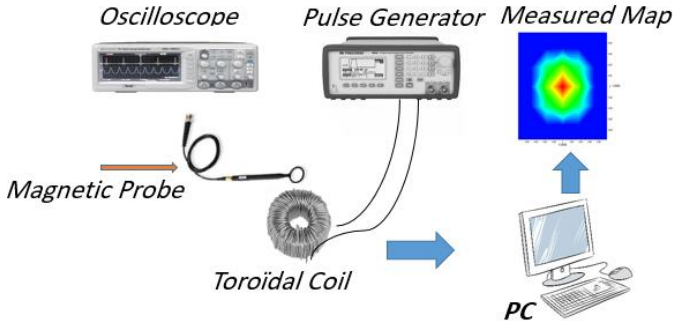
Fig. 9 *– Descriptive diagram of the near magnetic field measured above the inductance in the time domain.*

Fig. 10 – *Near magnetic field probe RSH-50-1 type: Rohde Schwarz.*

To measure the magnetic fields around electrical components and electronic systems, we can use magnetic probes, and to capture the different components of the magnetic field H. These probes are positioned with their normal aligned with the surface of the loop of the component under investigation. A single probe can be reoriented as needed depending on the component being measured. The underlying principle of the measurement protocol is based on Faraday and Lenz's law, which states that a varying magnetic field $F(t)$ passing through a closed circuit induces an electromotive force "*e*" across the loop. Expression (1) shows Faraday's law [29].

4 Impact of Pulse Signal Applied to Inductor

In another part, we compared the magnetic field over the toroidal inductor at the point $(x, y, z) = (3 \text{ cm}, 2 \text{ cm}, 0.5 \text{ cm})$ in both TD and FD. This allowed us to visualize the impact of frequency and voltage variations of the pulse signal on the magnetic field emitted by the toroidal inductor.

4.1 Impact of the frequency variation of the pulse signal

The pulse signal is widely used in switching power electronics switches to realize static converters such as choppers, inverters, etc. [30 − 33].

Fig. 11 shows pulse signals with amplitude of 5V, and a duty cycle set at 50% of the respective signal's frequency. To assess the impact of frequency, we examined the following frequencies: 500 kHz, 1 MHz and 1.5 MHz. Then, we quantified the radiations emitted by the magnetic component in both time and frequency domains. In one set of experiments, the amplitude Z above the inductor was varied, while in another set, a sweep was carried out on the surface of the inductor with a step of 0.5 cm.
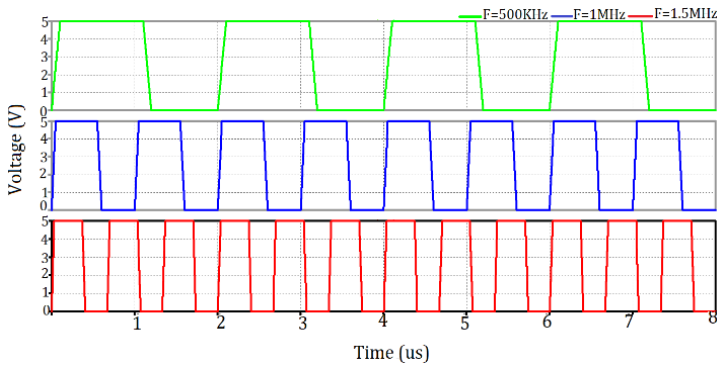

Fig. 11 − *Power supply signal to the inductor, by varying the pulse signal frequency.*

Fig. 12 shows the H_Z component of the near Magnetic field measured at the point $(x, y, z) = (3 \text{ cm}, 2 \text{ cm}, 0.5 \text{ cm})$ by the oscilloscope in the Time Domain (TD). We notice the peaks of radiated disturbances in the case of signal frequency $f = 1.5 \text{ MHz}$, then the peaks decrease with decreasing pulse frequency as shown in this figure.
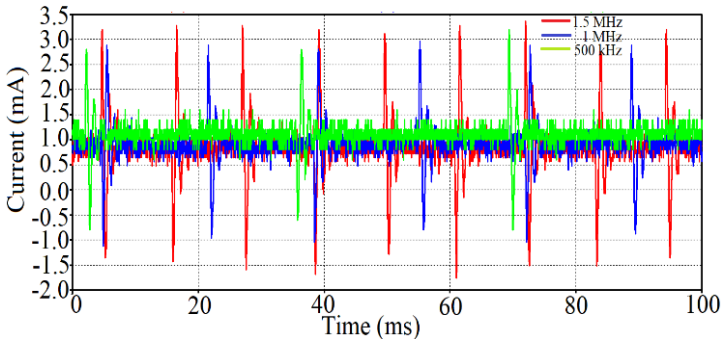

Fig. 12 − *H_Z of near Magnetic field measurement for different frequencies in time domain.*

Figs. 13, 14 and 15 show a comparison of the magnetic radiated emissions of all components H_X, H_Y, H_Z at the point $(x, y) = (3 \text{ cm}, 2 \text{ cm})$ between the time and frequency domains. This comparison is presented as a function of amplitude (Z) above the surface of the toroidal inductor. We notice a consistency between the values in the time and frequency domains for the three magnetic field components. In Fig. 13, which represents the component H_X, we observe that as the amplitude (Z) above the inductor increases, the magnetic field decreases. Hence, increase in signal frequency yields interesting magnetic emissions.
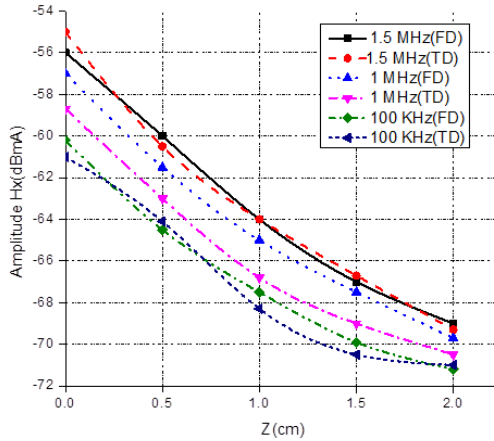

Fig. 13 – *H_X component of near Magnetic field at point $(x, y) = (3 \text{ cm}, 2 \text{ cm})$ as function of distance Z above the inductor in the time and frequency domain.*

Fig. 14 – *H_Y of near Magnetic field at point $(x, y) = (3 \text{ cm}, 2 \text{ cm})$ as function of distance Z above the inductor in the time and frequency domains.*
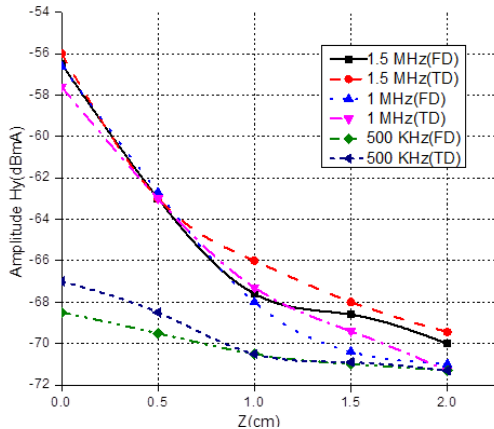
In Fig. 14, focusing on the component H_Y, we observe an interesting magnetic field behavior. This occurs when we either increase the signal frequency

or reduce the amplitude above the inductor, but it becomes prominent after a distance of $Z = 2$ cm. At that point, the emissions for all three signals become equal. In Fig. 15, representing the component H_Z, we observe similar patterns as in the other components. There is a consistent magnetic field agreement between the frequencies of 1 MHz and 1.5 MHz in both the time and frequency domains. Notably, the magnetic disturbances from the H_Z component emitted by the inductor are more significant, reaching values up to -40 dBmA at $Z = 0.5$ cm.
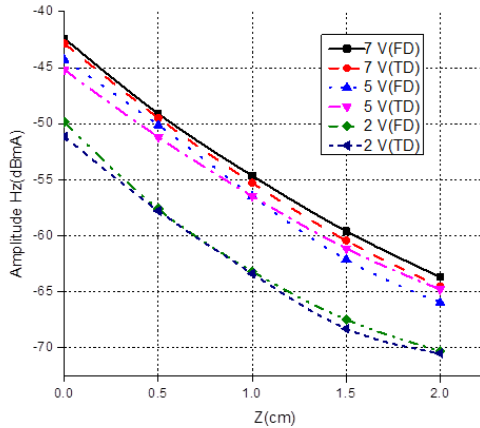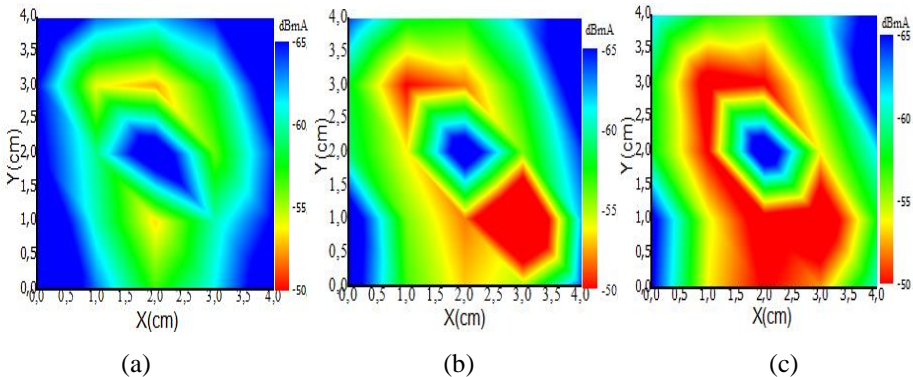

Fig. 15 – *H_Z of near Magnetic field at point* $(x, y) = (3cm, 2cm)$ *as function of distance Z above the inductor in the time and frequency domains.*

(a)   (b)   (c)

Fig. 16 – *Magnetic field maps of the H_Z component at surface* $(x, y) = (4cm, 4cm)$, *for Z = 0.5cm: (a) f = 500 kHz; (b) f = 1 MHz; (c) f = 1.5 MHz.*

Fig. 16 shows the magnetic field maps in the vicinity of component H_Z above the surface of the inductor at $Z = 0.5$ cm, as observed in the frequency domain for various pulse signal frequencies: 500 kHz, 1 MHz and 1.5 MHz. Notably, the maps reveal distinct radiation patterns. At a frequency of 1.5 MHz, the radiated emissions around the toroidal inductor appear significantly more pronounced,

denoted by the red color indicating values between -50 dBmA and -55 dBmA. However, these emissions decrease at the center and outside of the inductor as indicated by the blue color.

In contrast, when the pulse signal frequency is reduced to 500 kHz, the magnetic field around the inductor exhibits a decrease in intensity, evident in the green color on the frequency mapping. This indicates magnetic field amplitudes between -55 dBmA and -60 dBmA.

Fig. 17 shows H_X component of near magnetic field at point $(x, y, z) = (3\text{cm}, 2\text{cm}, 0.5 \text{ cm})$ above the inductor in the frequency domain. The measurements were taken for different pulse signals with a fixed voltage amplitude of 5V, and variable frequency as follows: $f = 50$ kHz, 500 kHz, 1.5 MHz and 3 MHz at the terminals of the toroidal inductor, with the same duty cycle of 50%. It is noticed that the radiated emissions at a frequency of 3MHz are higher and exhibit rapid oscillations compared to the other cases. These emissions exceed -54dBmA within the 50 MHz range, followed by a decrease in radiated disturbances towards higher frequencies.

Figs. 18 and 19 show, respectively, the H_Y and H_Z components. As can be clearly seen the amplitudes of the H_Z component exhibit a more pronounced increase compared to the H_X and H_Y components. This observation suggests the presence of the magnetic field initially in the Z direction and then in the Y direction. The field amplitude of the H_Z component exceeds -48 dBmA level for a 3 MHz frequency signal, approaching -48 dBmA in the H_Y component for the same pulse signal.

The magnetic field H_z exhibits greater intensity compared to the other components, H_X and H_Y, which is evident when comparing Figs. 17, 18 and 19. This difference is particularly noticeable for the signal frequency of 3 MHz, represented in black color. This suggests that the emitted field is more intense in the direction Z, followed by the Y direction and finally, the X direction.
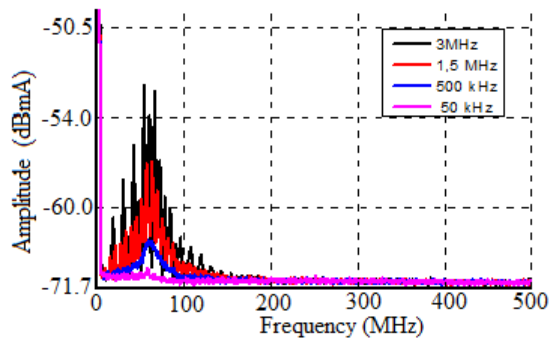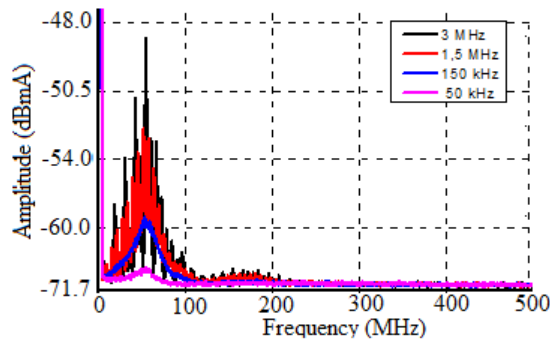

Fig. 17 – H_X *of the near magnetic field at the point*
$(x, y, z) = (3 \text{ cm}, 2 \text{ cm}, 0.5 \text{ cm})$ *above the inductor.*

Fig. 18 – H_Y *of the near magnetic field at the point*
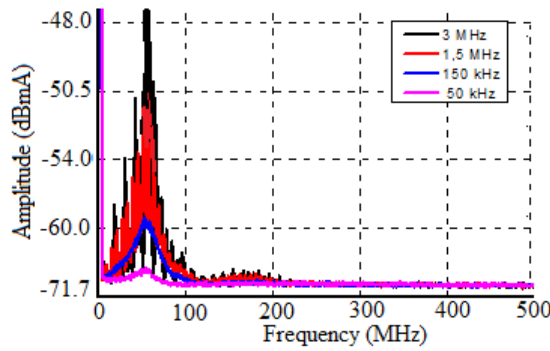*(x, y, z) = (3cm, 2cm, 0.5cm) above the inductor.*

Fig. 19 – H_Z *of the near magnetic field at the point*
(x, y, z) = (3 cm, 2 cm, 0.5 cm) above the inductor.

Table 1
Magnetic field in function of the frequency variation of all components.

Frequency		1,5 MHz			1 MHz			500 kHz		
Distance (cm)		**0,5**	**1**	**1,5**	**0,5**	**1**	**1,5**	**0,5**	**1**	**1,5**
Magnetic Field	H_x	-60,5	-64	-67	-63	-66,5	-69	-64	-68	-70,25
H (dBmA) Time	H_y	-63	-66	-78	-63	-67	-69	-69,5	-70	-71
Domain TD	H_z	-47,5	-53	-60	-50	-56	-61	-57	-62,5	-67,5
Magnetic Field	H_x	-60	-64	-67	-61,5	-65	-67,5	-64	-67,5	-69,75
H (dBmA) Frequency	H_y	-63	-68	-69,5	-63	-68	-70	-70,5	-70	-71
Domain FD	H_z	-47,5	-53	-59	-49	-56	-61,5	-57	-62,5	-67,5

Table 1 provides a summary of the magnetic field values for all the components as function of variations in frequency, distance between the surface of the coil inductor and the magnetic probe, in both the time and frequency domains. To ensure reliability, the reported values are derived from the average of three separate test measurement for each data point.

4.2 Impact of Amplitude variation on the pulse signal

In the second part of our study, we examine the impact of voltage pulse signals. Fig. 20 displays pulse signals at the terminals of the toroidal inductor, all having the same frequency 500 kHz and a duty cycle of 50%. We varied the amplitudes of voltage signals, considering values of 2 V, 5 V and 7V. This variation allows us to visualize the impact on the magnetic field components (H_X, H_Y, H_Z) in both time and frequency domains.

Fig. 21 shows the magnetic field of the H_Z component in the time domain for the three voltage values. One can clearly see that electromagnetic disturbances increase as the voltage applied to the inductor terminals increases. Conversely, reducing voltage amplitude results in a reduction of EMI peaks.
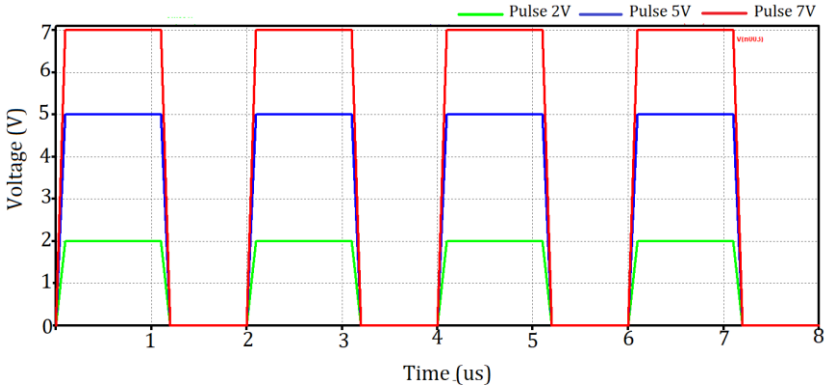

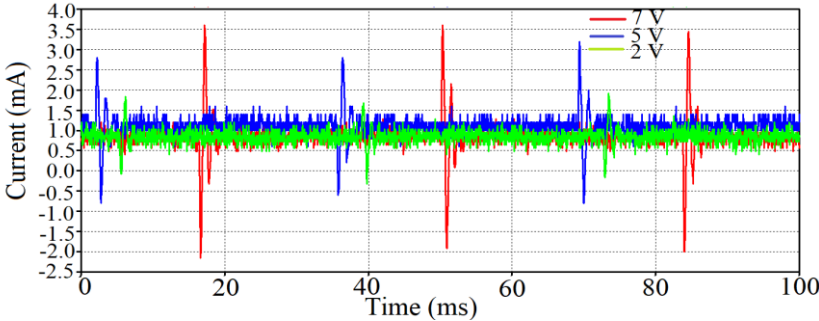**Fig. 20** − *Supply signal to the inductor with varied pulse signal amplitude.*

Fig. 21 − *H_Z of near magnetic field measured for different voltages in the time domain.*

Fig. 22 – H_X component of the magnetic field at the point $(x, y) = (3$ cm, 2 cm$)$ as function of distance Z over the inductor in the time and frequency domains.

Fig. 23 – H_Y component of the magnetic field at the point $(x, y) = (3$ cm, 2 cm$)$ as function of distance Z over the inductor in the time and frequency domains.

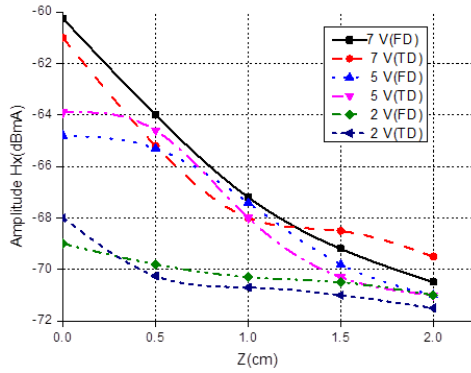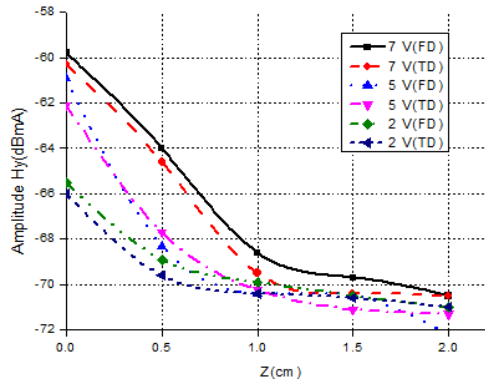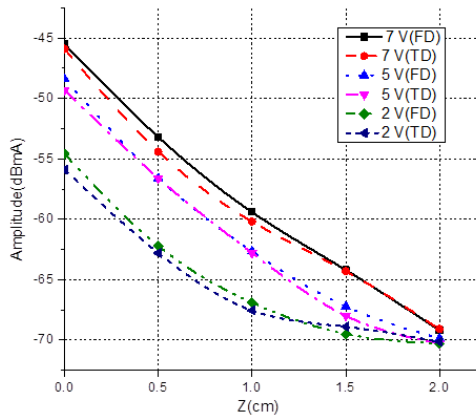**Fig. 24** – H_Z component of the magnetic field at the point $(x, y) = (3$ cm, 2 cm$)$ as function of distance Z over the inductor in the time and frequency domains.

Figs. 22, 23 and 24 provide a comparative analysis of the magnetic field for all components in both the time and frequency domains at point $(x, y) = (3$ cm, 2cm) as function of amplitude Z, representing the distance between the measurement point and the surface of the inductor. Notably, there is a strong concordance observed between the magnetic field patterns in these two domains. In Fig. 22, for the component H_X, we observe that radiated emissions decrease with increase in the amplitude Z. Additionally, there is a concordance between the magnetic field patterns for pulse signals with amplitudes of 5 V and 7 V after the distance $Z = 0.5$ cm from the magnetic probe to the inductor. Conversely, the 2V signal results in significantly weaker magnetic field emitted by the inductor.

Fig. 23 continues to demonstrate the concordance as it shows that after a distance $Z = 1$ cm, there reduction in magnetic field with either a decrease in signal voltage or an increase in amplitude Z. In Fig. 24, the magnetic emission of H_Z is significantly more pronounced than the other components, H_X, H_Y across all voltage amplitudes of the pulse signal. Furthermore, there is a concordance observed in the magnetic field patterns for the three pulse signals after the distance $Z = 2$ cm.

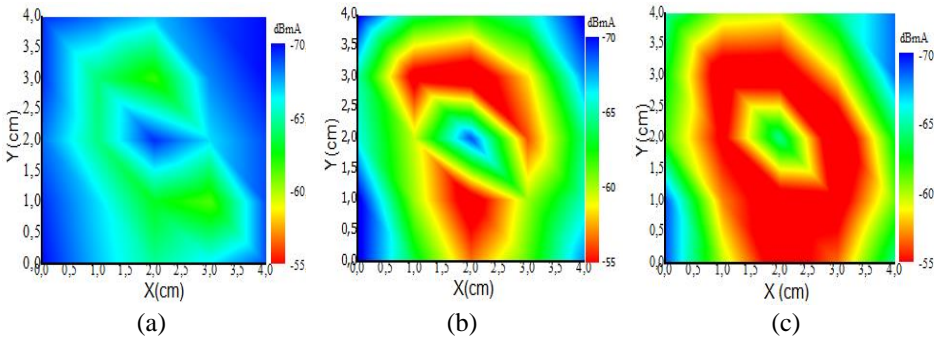(a)   (b)   (c)

Fig. 25 – *Magnetic field maps of the H_Z component at surface*
$(x, y) = (4$ cm, 4 cm) *above the inductor:* (a) 2V; (b) 5V; (c) 7V.

Fig. 25 shows the magnetic field maps of the *Hz* component in the range $[-55 \text{ dBmA}, -70 \text{ dBmA}]$ at the surface $(x, y) = (4$ cm, 4 cm), for different voltage amplitudes (2 V, 5V and 7 V), at the same frequency of 500 kHz with the same pulse signal duty cycle. The distance between the surface of the inductor and the measuring probe is $Z = 0.5$ cm.

Notably, the maps reveal "hot spots" surrounding the inductor, and "cold spots" at the center and outside of the inductance. With an increase in voltage amplitude, the magnetic field becomes significantly more intense, evident from the red color indicating values between -55dBmA and -60 dBmA. By contrast, the magnetic field decreases with decreasing amplitudes as demonstrated in Figs. 25a and 25b.
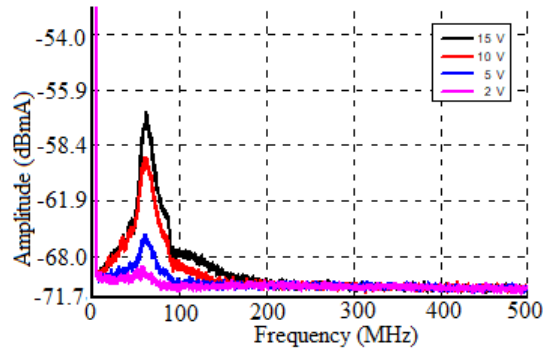
Fig. 26 – *Magnetic field of the component H_X at the point (x, y, z) = (3 cm, 2 cm, 0.5cm) above the inductor in frequency domain.*
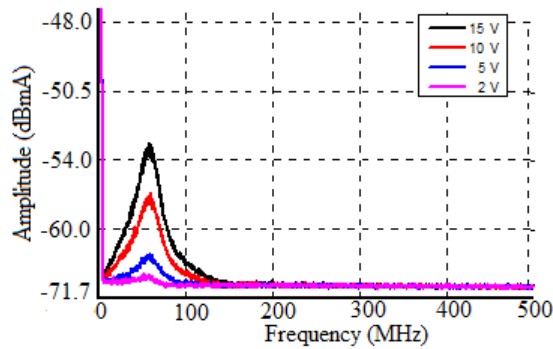

Fig. 27 – *Magnetic field of component H_X at point (x, y, z) = (3 cm, 2 cm, 0.5 cm) above the inductance in frequency domain.*

Fig. 26 illustrates the H_X component of the magnetic field at point (x, y, z) = (3 cm, 2 cm, 0.5 cm) above the inductor in the frequency domain observed with the aid of a spectrum analyzer. As can be observed in this figure, as we increase the voltage while maintaining the signal frequency fixed at 500 kHz, we observe an increase in the peaks of the magnetic field, particularly around 50MHz, followed by a reduction towards higher frequencies.

Fig. 27 shows the magnetic field of the H_Y component in the same point above the inductor for the different amplitudes (2 V, 5 V, 10 V and 15V). The results reveal peaks in radiated emissions followed by a reduction towards higher frequencies.

Fig. 28 displays the H_Z component of the magnetic field emitted by the inductor. Notably, the amplitudes of H_Z field are significantly larger than the other components, H_X, H_Y. This highlights the considerable influence of the signal voltage on the magnetic field, with more pronounced effect observed as the voltage of the pulse signal increases.
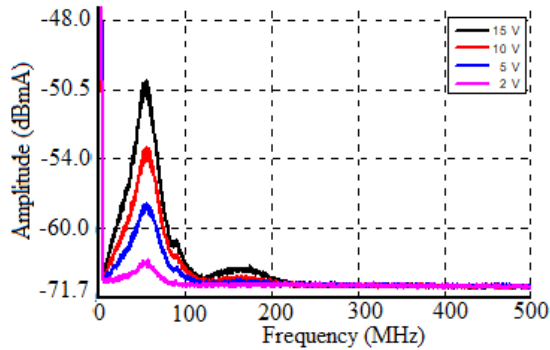
Fig. 28 – *Magnetic field of component H_Y at point $(x, y, z) = (3$ cm, 2 cm, 0.5 cm)*
above the inductor in frequency domain.

Based on the results obtained through the measurement of the near magnetic field emitted by the toroidal inductor using magnetic probes in both the time domain (TD) and frequency domain (FD), utilizing the oscilloscope and spectrum analyzer respectively, it can be concluded that there is a strong concordance between the two sets of results.

Table 2 summarizes the results obtained in both the time domain (oscilloscope) and the frequency domain (magnetic field spectrum analyzer) at the point $(x, y) = (3$ cm, 2 cm) as function of the voltage applied, and the distance between this point and the coil inductance. It is noteworthy that the frequency results have been validated through temporal analysis using Fourier transform, revealing a high degree of concordance between the two sets of results.

Table 2
Magnetic field in function of Voltage variation of all components.

Voltage		7 V			5 V			2 V		
Distance (cm)		0,5	1	1,5	0,5	1	1,5	0,5	1	1,5
Magnetic Field	H_x	-65	-68	-69,5	-64,5	-68	-70,5	-70	-70,5	-71
H (dBmA) Time	H_y	-64	-69,5	-70,5	-68	-70	-70,5	-69	-70,5	-70,5
Domain TD	H_z	-55	-60	-64,5	-56	-62,5	-67,5	-62,5	-67,5	-70
Magnetic Field	H_x	-64	-67	-69,5	-65	-68	-70	-70	-70,5	-70,5
H (dBmA) Frequency	H_y	-64	-68,5	-70	-68	-70	-70,5	-69,5	-70,5	-71
Domain FD	H_z	-54	-60	-64,5	-56	-62,5	-67,5	-62,5	-67,5	-70

5   Conclusion

The near field survey method is widely employed to quantify the radiated emissions produced by electronic power systems.

In this paper, we have quantified the radiated emissions generated by the toroidal coil in the frequency domain (FD) and time domain (TD) across three directions: *X, Y* and *Z*. We have also examined the impact of frequency and voltage amplitude of the pulse signal applied to the inductor terminals on the magnetic field, as well as the effect of the of the distance *Z* between the measurement point and the magnetic component. Our findings reveal that pulse signals used for controlling power electronic switches and static converters, including their amplitudes and switching frequencies, and duty, have a significant impact not only on conducted electromagnetic interference (EMI) but also on radiated emissions. This impact is particularly evident in the inductor, a primary source of magnetic field emissions. These measurements are relevant for test laboratories.

In future research, we plan to explore methods for reducing the magnetic field emitted by the inductor through magnetic shielding. We aim to determine the shielding efficiency as function of voltage and frequency.

6   Acknowledgements

7   References

[1]   I. B. Mahamat, D. A. Oumar, S. Malloum, D. Pietroy, S. Capraro, J. P. Chatelon, J. J. Rousseau: Magnetic Field Radiated by Iintegrated Inductors and Magnetic Shielding, Proceedings of the IEEE International Conference on Industrial Technology (ICIT), Lyon, France, February 2018, pp. 747 – 752.

[2]   L. Decrock, J. Catrysse, F. Vanhee, D. Pissoort: Measuring and Simulating EMI on Very Small Components at High Frequencies, Proceedings of the International Symposium on Electromagnetic Compatibility, Brugge, Belgium, September 2013, pp. 961 – 965.

[3]   A. Zeghoudi, A. Bendaoud, A. Tilmatine, S. Bechkir, G. Zissis, L. Canale: Study of the Impact of the Power Dimming and Lighting Modes of LED Lamps on the Near Magnetic Field, Optik, Vol. 271, December 2022, p. 169997.

[4]   M. A. Chahine, M. Khatib, A. Hamié, R. Perdriau, M. Ramdani: Near Field Measurement System for the Detection of Electromagnetic Field Components Radiated by Microwave Devices, in Microwave Symposium (MMS), Proceedings of the 13th Mediterranean Microwave Symposium (MMS), Saida, Lebanon, September 2013, pp. 1 – 4.

[5]   A. Zeghoudi, A. Bendaoud, H. Slimani, M. Miloudi, H. Miloudi, L. Canale: Experimental Measurements of Near Magnetic Field by Different Probe for AC/DC LED Driver, Proceedings of the IEEE International Conference on Environment and Electrical Engineering and IEEE Industrial and Commercial Power Systems Europe (EEEIC/ICPS Europe), Prague, Czech Republic, June 2022, pp. 1 – 6.

[6] H. Shall, Z. Riah, M. Kadi: Prediction of 3D-Near Field Coupling Between a Toroidal Inductor and a Transmission Line, Proceedings of the IEEE International Symposium on Electromagnetic Compatibility, Denver, USA, August 2013, pp. 651 – 656.

[7] S. Orlandi, B. Allongue, G. Blanchot, S. Buso, F. Faccio, C. Fuentes, M. Kayal, S. Michelis, G. Spiazzi: Optimization of Shielded PCB Air Core Toroids for High Efficiency DC-DC Converters, Proceedings of the IEEE Energy Conversion Congress and Exposition, San Jose, USA, November 2009, pp. 2073 – 2080.

[8] A. Zeghoudi, A. Bendaoud, H. Miloudi, S. Bechkir, H. Slimani, M. Miloudi: Effectiveness of Shielding on the Magnetic Emissions Emitted by the Toroidal Inductor, Proceedings of the 2nd International Conference on Advanced Electrical Engineering (ICAEE), Constantine, Algeria, October 2022, pp. 1 – 7.

[9] Y. Chu, S. Wang, N. Zhang, D. Fu: A Common Mode Inductor with External Magnetic Field Immunity, Low-Magnetic Field Emission, and High-Differential Mode Inductance, IEEE Transactions on Power Electronics, Vol. 30, No. 12, December 2015, pp. 6684 – 6694.

[10] Y. Chu, S. Wang, J. Xu, D. Fu: EMI Reduction with Near Field Coupling Suppression Techniques for Planar Transformers and CM Chokes in Switching-Mode Power Converters, Proceedings of the IEEE Energy Conversion Congress and Exposition, Denver, USA, September 2013, pp. 3679 – 3686.

[11] S. Wang, F. C. Lee, W. G. Odendaal, J. D. van Wyk: Improvement of EMI Filter Performance with Parasitic Coupling Cancellation, IEEE Transactions on Power Electronics, Vol. 20, No. 5, September 2005, pp. 1221 – 1228.

[12] S. Wang, R. Chen, J. D. van Wyk, F. C. Lee, W. G. Odendaal: Developing Parasitic Cancellation Technologies to Improve EMI Filter Performance for Switching Mode Power Supplies, IEEE Transactions on Electromagnetic Compatibility, Vol. 47, No. 4, November 2005, pp. 921 – 929.

[13] S. Wang, F. C. Lee, J. D. van Wyk: Design of Inductor Winding Capacitance Cancellation for EMI Suppression, IEEE Transactions on Power Electronics, Vol. 21, No. 6, November 2006, pp. 1825 – 1832.

[14] A. Hariya, T. Koga, K. Matsuura, H. Yanagi, S. Tomioka, Y. Ishizuka, T. Ninomiya: Circuit Design Techniques for Reducing the Effects of Magnetic Flux on GaN-HEMTs in 5-MHz 100-W High Power-Density LLC Resonant DC–DC Converters, IEEE Transactions on Power Electronics, Vol. 32, No. 8, August 2017, pp. 5953 – 5963.

[15] J. Yao, S. Wang, Z. Luo: Modeling, Analysis, and Reduction of Radiated EMI Due to the Voltage Across Input and Output Cables in an Automotive Non-Isolated Power Converter, IEEE Transactions on Power Electronics, Vol. 37, No. 5, May 2022, pp. 5455 – 5465.

[16] J. Yao, Y. Li, S. Wang, X. Huang, X. Lyu: Modeling and Reduction of Radiated EMI in a GaN IC-Based Active Clamp Flyback Adapter, IEEE Transactions on Power Electronics, Vol. 36, No. 5, May 2021, pp. 5440 – 5449.

[17] J. Yao, Y. Li, H. Zhao, S. Wang, Q. Wang, Y. Lu, D. Fu: Modeling and Reduction of Radiated Common Mode Current in Flyback Converters, Proceedings of the IEEE Energy Conversion Congress and Exposition (ECCE), Portland, USA, September 2018, pp. 6613 – 6620.

[18] Y. Zhang, S. Wang, Y. Chu: Investigation of Radiated Electromagnetic Interference for an Isolated High-Frequency DC–DC Power Converter with Power Cables, IEEE Transactions on Power Electronics, Vol. 34, No. 10, October 2019, pp. 9632 – 9643.

[19] J. He, Z. Guo, X. Li: Mechanism Model and Prediction Method of Common Mode Radiation for a Nonisolated Very-High-Frequency DC–DC Converter with Cables, IEEE Transactions on Power Electronics, Vol. 35, No. 10, October 2020, pp. 10227 – 10237.

[20] W. Labiedh, B. Zitouna, M. Tlig, J. B. Hadj Slama: Development of Generic Radiating Model for Rectangular Capacitors: Magnetic Near Fields Analysis and Modeling, Ch. 13, Recent Topics in Electromagnetic Compatibility, IntechOpen, London, 2021.

[21] S. Hedia, B. Zitouna, J. B. Hadj Slama, L. Pichon: Electromagnetic Time Reversal in the Near Field: Characterization of Transient Disturbances in Power Electronics, IEEE Transactions on Electromagnetic Compatibility, Vol. 62, No. 5, October 2020, pp. 1869 – 1878.

[22] S. Hedia, B. Zitouna, J. B. Hadj Slama, L. Pichon: A Full Time Domain Methodology Based on Near Field Time Reversal for Equivalent Source Identification, Proceedings of the IEEE International Symposium on Electromagnetic Compatibility and IEEE Asia-Pacific Symposium on Electromagnetic Compatibility (EMC/APEMC), Suntec City, Singapore, May 2018, pp. 141 – 146.

[23] F. Benyoubi, L. Pichon, M. Bensetti, Y. Le Bihan, M. Feliachi: An Efficient Method for Modeling the Magnetic Field Emissions of Power Electronic Equipment from Magnetic Near Field Measurements, IEEE Transactions on Electromagnetic Compatibility, Vol. 59, No. 2, April 2017, pp. 609 – 617.

[24] L. Beghou, B. Liu, L. Pichon, F. Costa: Synthesis of Equivalent 3-D Models from Near Field Measurements–Application to the EMC of Power Printed Circuit Boards, IEEE Transactions on Magnetics, Vol. 45, No. 3, March 2009, pp. 1650 – 1653.

[25] W. K. Chen: The Electrical Engineering Handbook, Elsevier Academic Press, Amsterdam, Boston, London, 2005.

[26] J.- C. Bolomey, F. E. Gardiol: Engineering Applications of the Modulated Scatterer Technique, Artech House, Boston, London, 2001.

[27] S. A. Boulingui: Etude du couplage électromagnétique entre circuits intégrés par émulation du perturbateur - Application en téléphonie 3G, Ph.D. Thesis, Université de Toulouse, Toulouse, 2009.

[28] R&S®HZ-15/R&S®HZ-17 Probe Sets R&S®HZ-16 Preamplifier: E and H near-field emission measurements with test receivers, spectrum analyzers and oscilloscopes, Product Brochure version 01.00.

[29] B. Zitouna, J. B. Hadj Slama: An Efficient Approach Based on the Near Field Technique to Solve EMI Problems: Application to an AC/DC Flyback Converter, Ch. 8, Advances in Complex Analysis and Applications, IntechOpen, London, 2020.

[30] H. Slimani, A. Zeghoudi, A. Bendaoud, A. Reguig, B. Benazza, N. Benhadda: Experimental Measurement of Conducted Emissions Generated by Static Converters in Common and Differential Modes, European Journal of Electrical Engineering (EJEE), Vol. 23, No. 3, June 2021, pp. 273 – 279.

[31] H. Slimani, A. Zeghoudi, A. Bendaoud, S. Bechekir: Experimental Evaluation of Conducted Disturbances Induced During High Frequency Switching of Active Components, Electrical Engineering and Electromechanics, No. 5, August 2023, pp. 26 – 30.

[32] A. Zeghoudi, A. Bendaoud, H. Slimani, B. Benazza, D. Benouna: Determination of Electronics Disturbances in a Buck Chopper, Australian Journal of Electrical and Electronics Engineering, Vol. 19, No. 2, January 2022, pp. 149 – 157.

[33] A. Zeghoudi, A. Bendaoud, H. Slimani, H, Miloudi, M. Miloudi, N. Chikhi: Experimental Measurement of Common and Differential Modes for Variable Speed Drive DC Motor, Proceedings of the 19th International Multi-Conference on Systems, Signals & Devices (SSD), Setif, Algeria, May 2022, pp. 532 – 537.